Effects of annealing on the optical properties of $AgIn_{0.8}Ga_{0.2}Se_2$ thin films

F. CHOWDHURY [*,a], J. BEGUM[a], M. S. ALAM[b,c], S. M. F. HASAN[a]
[a]*Experimental Physics Division, Atomic Energy Centre, Bangladesh Atomic Energy Comission, 4, Kazi Nazrul Islam Avenue, Dhaka-1000*
[b]*Department of Physics, University of Dhaka, Ramna, Dhaka-1000, Bangladesh*
[c]*Department of Physics, University of Erlangen-Nuremberg, Erwin-Rommel Strasse 1, D-91058 Erlangen, Germany*

Silver indium gallium di-selenide ($AgIn_{0.8}Ga_{0.2}Se_2$) quaternary thin films have been grown onto ultrasonically and chemically cleaned glass substrates by three and four stage Stacked Elemental Layer Deposition (SEL) process. The stack of successively evaporated individual elemental layers was annealed in situ in the temperature ranging between 200°C and 350°C, for 15 min. Optical properties of the films have been ascertained by UV-VIS-NIR spectrophotometry (photon wavelength ranging between 300 and 2500 nm). The sharp descent of the transmission spectra reveals standard semiconducting nature that confirms the microstructural perfection of the films. Tuning of band gap is achieved for future tandem solar cells and various photovoltaic applications. The optical absorption behaviour above the fundamental absorption edge can be interpreted by considering the existence of at least two types of transitions: direct allowed and direct forbidden transitions. The former varies from 1.172 to 1.264 eV and the later varies as 1.49 to 1.67 eV, depending on annealing temperatures. Spin-orbit splitting of valence band due to spin-orbit interaction of electrons decreases with the increasing of annealing temperatures. The surface topography was studied at nanometric scale by atomic force microscopy (AFM). Urbach energy shows a minimum value at 300 °C.

(Received October 30, 2010; accepted November 29, 2010)

Keywords: $AgIn_{0.8}Ga_{0.2}Se_2$ thin film, Four stage film, Optical properties, Spin-orbit splitting, Urbach energy

1. Introduction

$CuIn(Ga)Se_2$ (CIGS) is one of the most promising chalcopyrite materials for commercial photovoltaic applications [1-5]. Recently, the conversion efficiencies of polycrystalline thin film solar cells based on $Cu(In,Ga)Se_2$ has reached a value 19.9 % by modifying the CIGS surface and making it look like $CuInSe_2$ (CIS) [6-8]. However, a shortcoming of $Cu(In_{1-x},Ga_x)Se_2$ thin film solar cells is that the efficiency decreases as the band gap energy (E_g) increases above 1.3 eV [9]. CIGS solar cell has short wavelength absorption properties due to its relatively small band gap of 1.1 eV, which plays negative impact in its application in photovoltaic devices. Apart from that, copper causes shorting effects in photovoltaic devices due to its larger diffusion coefficient. One way of improving the higher conversion efficiency is by stacking cells of different band gaps in series; that is a tandem structure. We, therefore, investigate the optical properties of $AgIn_{0.8}Ga_{0.2}Se_2$ (AIGS) thin films as a top cell for tandem solar cells in the present study. The band gap energy of AIGS is larger than that of CIGS by 0.2 eV [10], and the melting point is lower than that of CIGS by 200 °C. To our knowledge, studies on the optical properties of chalcopyrite quaternary compound $AgIn_{0.8}Ga_{0.2}Se_2$ have not been studied before [11-13]. In the present work, indium (In) has been incorporated to AGS_2 thin film for assessing its potentiality for solar cell applications. Films were developed thermally by three and four stages stacked elemental layer (SEL) deposition process. Our studies on three stage $AgIn_{0.8}Ga_{0.2}Se_2$ films have been reported elsewhere [14]. We will concentrate on our investigations on four stage $AgIn_{0.8}Ga_{0.2}Se_2$ thin films in this paper after addressing a comparative view of three and four stage $AgIn_{0.8}Ga_{0.2}Se_2$ films.

2. Experimental

2.1. Growth of the films

$AgIn_{0.8}Ga_{0.2}Se_2$ thin films of silver (Ag), indium (In), gallium (Ga) and selenium (Se) were deposited sequentially onto chemically and ultrasonically cleaned glass substrates by thermal evaporation of individual elemental layers to form a stack, in vacuum ($\approx 10^{-7}$ mbar) using an oil diffusion pump (E 306A, Edwards, UK). The rate of deposition was 0.2 nm/sec, 0.3 nm/sec, 0.8 nm/sec and 0.3 nm/sec for Ga, In, Se and Ag, respectively. Thicknesses of individual layers to be deposited were calculated prior to the preparation of the films. During preparation, the thicknesses were measured *in situ* by frequency shift of FTM5 quartz crystal thickness monitor (Edwards, UK); which also monitors the rate of deposition. The stack of elements on the substrate was thermally annealed *in situ* at temperatures ranging between 200 °C and 350 °C, for 15 min to facilitate the degrees of

freedom of the elemental atoms to arrange among themselves. Thickness of all films was kept fixed at 500±10 nm.

2.2. Optical measurements

2.2.1. Transmittance, reflectance and thickness

Optical transmittance (T) and absolute specular reflectance (R) of the films with wavelength of light incident on them were measured using a dual-beam UV-VIS-NIR recording spectrophotometer (Shimadzu, UV-3100, Japan) in the photon wavelength range between 300 and 2500 nm. Light signals coming from the samples were detected by an integrating sphere. The thickness of the composite films was checked by the infrared interference method, utilizing the spectrophotometer. It depends on the reflectance characteristics of the films. In this method the thickness of a film is given by

$$d = \frac{\Delta m}{2\sqrt{n_1^2 - \sin^2\theta}} \frac{1}{(1/\lambda_1) - (1/\lambda_2)} \qquad (1)$$

where n_1 is the refractive index of the film, θ is the incident angle of light to the sample, λ_1 and λ_2 are the peak or valley wavelengths in the reflectance spectrum and Δm is the number of peaks or valleys between λ_1 and λ_2, where $\lambda_2 > \lambda_1$. The thickness was calculated using a fixed value of n_1 (here, $n_1 = 2.70$). The obtained thickness of the films was 500 ± 10 nm which conforms with the measuring value of thickness monitor as was controlled during experiment.

2.2.2. Absorption coefficient and band gap energy.

Expression for the multiple- reflected systems has been given by Heavens for transmittance (T%) at normal incidence and reflectance (R%) at near-normal incidence of light on the films [15]. Tolmin [16] simplified this expression for absorbing films on non-absorbing substrates and expressed it as

$$\frac{1-R}{T} = \frac{1}{2n_2}(n_1^2 + k_1^2) \times \left[n_1\{(n_1^2 + n_2^2 + k_1^2)\sinh 2\alpha_1 + 2n_1 n_2 \cosh 2\alpha_1\} + k_1\{n_1^2 - n_2^2 + k_1^2)\sin 2\gamma_1 + 2n_2 k_1 \cos 2\gamma_1\}\right] \qquad (2)$$

Where, n_1 and n_2 are the refractive indices of the film and substrate, respectively. k_1 is the extinction coefficient of the film. $\alpha_1 = 2\pi k_1 d/\lambda$, $\gamma_1 = 2\pi n_1 d/\lambda$, where d is the thickness of the film and λ is the wavelength of light. This equation has been solved for k_1 using a computer iteration process, n_2 = 1.45. Absorption coefficient α was calculated by using the relationship $\alpha = 2\pi kd/\lambda$. The band gap energy has been calculated by using the above mentioned model from the dependence of absorption coefficient, on photon energy. Dependence of α on photon energy will be analyzed with the existing models discussed in Eqs. (3) and (4) to find the nature and extent of the band gap energy.

2.3. Atomic Force Microscopy (AFM) measurements

The surface topography of the investigated sample was studied by Atomic Force Microscopy (AFM) technique. All AFM images were recorded using a NT-MDT instrument operating in non-contact mode. Resolution for topography measurements was 256 × 256 points. The experiment was carried out under ambient condition.

3. Results and discussion

Fig. 1 demonstrates the comparison of optical transmission spectra between three and four stage $AgIn_{0.8}Ga_{0.2}Se_2$ thin films annealed in situ at different temperatures from 200 °C to 350 °C. From the abruptness of the reduction in the transmittance pattern it is clear that the quaternary compound of

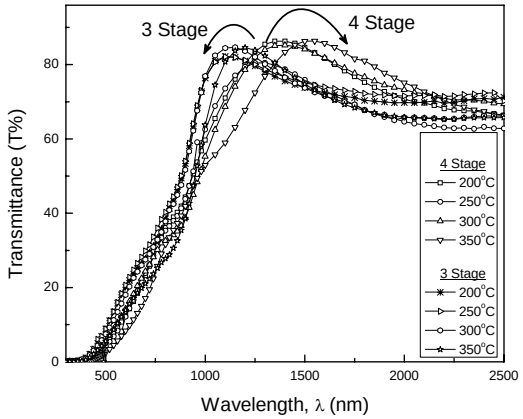

Fig. 1. Comparison between the optical transmittance of three and four stage $AgIn_{0.8}Ga_{0.2}Se_2$ thin films at different annealing temperatures as a function of photon wavelength.

AIGS is formed at all the compositions. The four stage films spectra shifts towards the higher photon wavelength regime and, thereby by lowering the band gap. In both three and four stage cases, the films attain perfect semiconducting properties at 300 °C, which indicates adherence to the best formation of the compound. Since it is observed that the absorption regions for these films are steeper that has more distinct absorption edge than those of other films. We now will continue with our investigations on four stage films throughout the rest of this paper. Absorption spectrum as a function of photon energy for four stage film annealed at 300 °C is shown in Fig. 2 (a). Films annealed at 200 °C and 350 °C show tail absorptions. Tail absorption results from the departure of the lattice from perfect periodicity that causes lattice

imperfections. Grain boundary disorder also creates unexpected localized states within the band gap. Width of the localized states represented by Urbach energy, E_U (minimum value at 300 ^oC) will be discussed later in this paper.

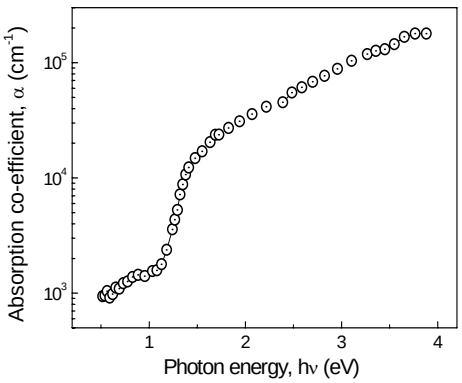

(a)

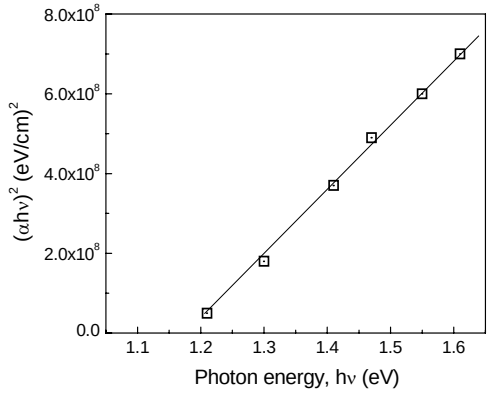

(b)

Fig. 2. (a) Dependence of absorption coefficient on photon energy for four stage $AgIn_{0.8}Ga_{0.2}Se_2$ thin films annealed at 300 ^oC. (b) Typical dependence of the parameter $(\alpha h\nu)^2$ on photon energy, hν.

Tail absorption is insignificant for the film with annealing temperature of 250^{o}C and 300^{o}C implying that these films are free from lattice imperfections. The analysis of the absorption coefficient, α above the fundamental edge has high values as high as10^5 cm^{-1} and the rise of α in the photon energy range $1.170 \le \alpha \le 1.265$ eV follows a relation for an allowed direct interband transition [17] described by

$$\alpha = \frac{A_1}{h\nu}\left[h\nu - E_{g1} \right]^{1/2} \qquad (3)$$

where E_{g1} is the band gap energy of the interband transition and A_1 is a parameter that depends on the probability of transition and the refractive index of the material. The values of electron transition energy E_{g1}, and A_1 were extracted from the plot of $(\alpha h\nu)^2$ versus hν (Fig. 2(b)). Direct allowed transitions vary between 1.172 and 1.264 eV, giving a reasonable value which lies below the band gap value of AGS thin film (1.8 eV) [18]. The band gap energy decreases as the annealing temperature increases. The interatomic spacing increases when the amplitude of the atomic variation increases due to the increased thermal energy. An increased intertomic spacing decreases the potential seen by the electrons in the material; and thus reducing the band gap energy. If we now calculate the absorption coefficient for hν >1.45 eV by putting the obtained values of E_{g1} and A_1, in Eq. (3) and called it α_1 (theoretical α), then we find that α_1 is smaller than the experimentally measured absorption coefficient, α (Fig. 3 (a)). This discrepancy can only be explained by assuming an additional absorption $\alpha_2 = \alpha - \alpha_1$, above 1.45 eV of photon energy. The additional absorption curve (α_2) is further analyzed and it was found that it follows the relation for direct forbidden interband transition for $1.45 \le \alpha \le 1.69$ eV described by

$$\alpha = \frac{A_2}{h\nu}\left[h\nu - E_{g2} \right]^{3/2} \qquad (4)$$

The forbidden energy gap E_{g2} and the parameter A_2 were calculated from the plot of $(\alpha_2\ h\nu)^{2/3}$ versus hν as shown in Fig. 3 (b). The calculated optical values are shown in Table 1.

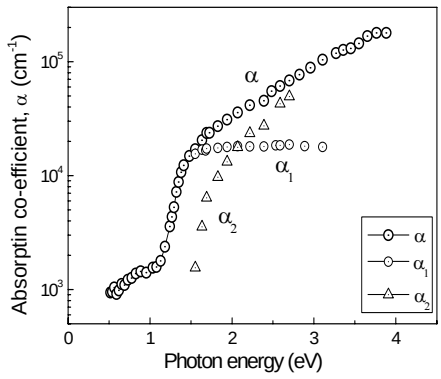

(a)

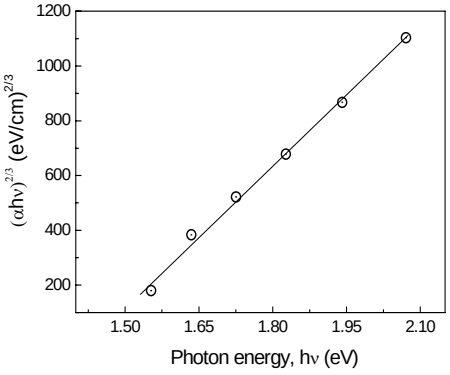

(b)

Fig. 3. (a) Comparison of the theoretically calculated and experimentally measured optical absorption coefficients as a function of photon energy for four stage $AgIn_{10.8}Ga_{0.2}Se_2$ thin films. (b) Typical dependence of the parameter $(\alpha_2 h\nu)^{2/3}$ on photon energy, hν.

Crystal field splitting Δ_{cf} is not found in the analysis, as in that case we would obtain a transition energy slightly higher than E_{g1}. Hence, the spin–orbit splitting has been calculated from the difference between E_{g1} and E_{g2}, putting Δ_{cf} to be zero in the model of Shay and Rowe [19]. Variation of energy gaps (direct allowed and forbidden) and spin–orbit splitting on annealing temperatures are plotted in Fig. 4. It is depicted from the figure that the dependence of direct allowed energy gap on annealing temperatures has correlation with the dependence of spin–orbit splitting in the temperature range between 250 ^{o}C and 350 ^{o}C. Wheras, direct forbidden gap follows this correlation for the entire temperature range. This similarity indicates that splitting of the valence band due to spin–orbit interaction of the electrons acts as an origin of direct forbidden energy gap. Fig. 5 shows the AFM image for $AgIn_{10.8}Ga_{0.2}Se_2$ thin film annealed at 300 ^{o}C by 2 and 3-D scanning; which is considered to be the best film regarding its optical investigations. The AFM topography revealed the granular nature of the film. The grains are densely packed. The rms (root mean square) values of the roughness estimated from the AFM image is ~50 nm.

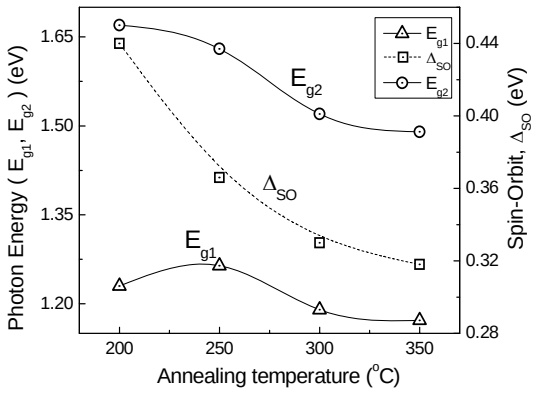

Fig. 4. Dependence of energy gaps (E_{g1} and E_{g2}) and spin–orbit splitting on annealing temperature of four stage $AgIn_{10.8}Ga_{0.2}Se_2$ thin films.

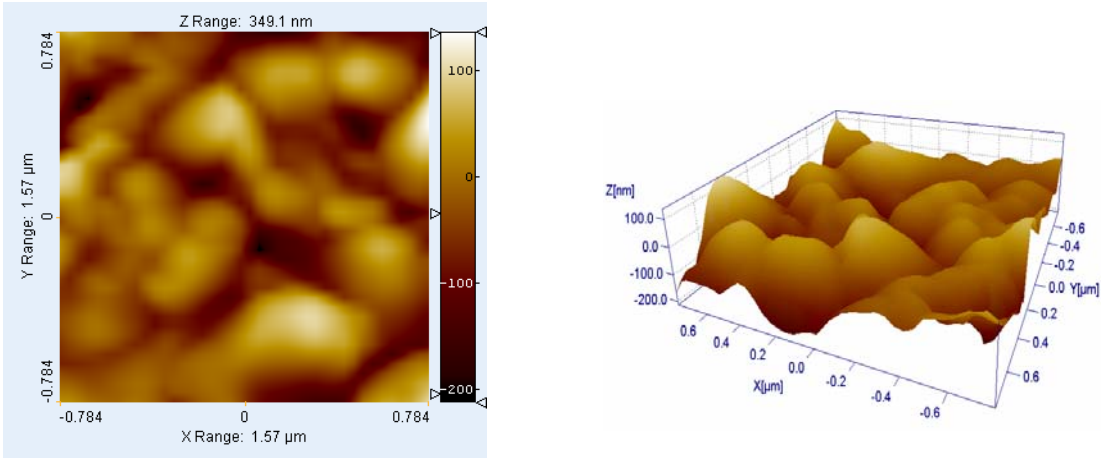

(a) (b)

Fig. 5. (a) 2-D and (b) 3-D AFM image on 1.6 × 1.6 µm^2 area of four stage $AgIn_{0.8}Ga_{0.2}Se_2$ thin film annealed at 300 ^{o}C.

Width of the localized states can be expressed by the Urbach energy (E_U) which can be obtained from the following relation

$$\alpha = \alpha_o \exp(h\nu/E_U)$$

where α_o is a constant. Values of E_U were calculated from the slope of ln α versus energy (hν).

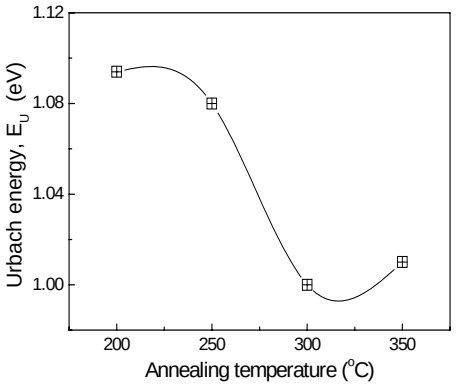

Fig. 6. Urbach energy (E_u) of four stage $AgIn_{0.8}Ga_{0.2}Se_2$ thin film as a function of annealing temperature.

Urbach energy is plotted as a function of annealing temperature in Fig. 6. It is observable that the Urbach energy has a general tendency to decrease with the increase of annealing temperature; indicating the decrease in the width of the localized states.

4. Conclusions

$AgIn_{0.8}Ga_{0.2}Se_2$ thin films of desired optical quality could be grown. The band gap could be tuned successfully by varying stage of film formation, annealing temperature for optimized use of this material in future tandem solar cell applications. Splitting of valence band due to spin-orbit interaction of electrons appears as an origin of direct forbidden bandgap. Critical analysis on the optical absorption coefficients was assigned as high as 10^5 cm^{-1}, above the fundamental absorption edge. AFM study shows granular nature of the film. Urbach energy has a general tendency to decrease with increasing annealing temperatures and thereby, decreasing the width of localized state. Film annealed at 300^{o}C shows sharp descent in the absorption spectra and lowest Urbach energy.

Acknowledgements

The authors are thankful to Mr. Syed Ayubur Rahman and Mrs. Jahanara Parvin and Mr. Ali Ahmed for their assistance in preparing the samples.

References

[1] M. J. Romero, K. M. Jones, J. AbuShama, Y. Yan, M. M. Al-Jassim, R. Noufi, Appl. Phys. Lett. **83**, 4731 (2003).
[2] F. B. Dejene, V. Alberts, J. Phys. D: Appl. Phys. **38**, 22 (2005).
[3] F. Long, W. Wang, J. Du, Z. Zou, J. of Physics: Conference Series **152**, 012074 (2009).
[4] A. I. Dirnstorfer, D. M. Hofmann, D. Meister, B. K. Meyer, J. of Appl. Phys. **85**, 1423 (1999).
[5] D. Young, M. Romero, W. Metzger, R. Noufi, J. Ward, A. Duda, Prog. Photovoltaics, **10**, 445 (2003).
[6] I. Repins, Contreras, A. Miguel, Egaas, Brian Dehart, Clay, Scharf, John; Perkins, L. Craig. To, Bobby; Noufi, Rommel, Prog. in Photovoltaics: Research and applications **16**, 235 (2008).
[7] S. M. Firoz Hasan, M. A. Subhan, Kh. M. Mannan, Optical Materials, **14**, 329 (2000).
[8] S. M. Firoz Hasan, L. Quadir, Kh. S. Begum, M. A. Subhan, Kh. M. Mannan, Sol. Energy Mater. & Sol. Cells, **58**, 349 (1999).
[9] R. Herberholtz, V. Nadnau, U. Ruhle, C. Ko¨ble, H. W. Schock, B. Dimmler, Solar Ener. Mat. and Solar Cells, **49**, 227 (1997).
[10] H. J. Moller, Semiconductor for solar cells, Artech House, Boston p. 292 (1993).
[11] K. Yamada, N. Hoshino, T. Nakada, Science and Techn. of Adv. Mat, **7**, 42 (2006).
[12] T. Nakada, K. Yamada, R. Arai, H. Ishizaki, N. Yamada, Mater. Res. Soc. Symp. Proc. 865 (2005) Materials research Society.
[13] H. Ishizaki, K. Yamada, R. Arai, Y. Kuromiya, Y. Masatsugu, N. Yamada, T. Nakada, Mater. Res. Soc. Symp. Proc. 865 (2005) Materials research Society.
[14] F. Chowdhury, J. Begum, S. M. Firoz Hasan, In progress, Submitted to Thin Solid Films.
[15] O. S. Heavens, Opt. Prop. of Thin Solid Films, (1965) (London: Butterworth).
[16] S. G. Tomlin, J. Phys. D: Appl. Phys. **1**, 667 (1968).
[17] S. M. Patel, V. G. Kapale, Thin Solid films, **148**, 143 (1987).
[18] H. Matsuo, K. Yoshino, T. Ikari, phys. stat. sol. (c) **3**, (8), 2639 (2006).
[19] J. E. Rowe, J. L. Shay, Phys. Rev. B, **3**, 451 (1971).

*Corresponding author: farzanaaktar97@yahoo.com